ISSN 1995-0780, Nanotechnologies in Russia, 2020, Vol. 15, Nos. 11–12, pp. 778–784. © Pleiades Publishing, Ltd., 2020.
Russian Text © The Author(s), 2020, published in Rossiiskie Nanotekhnologii, 2020, Vol. 15, No. 6, pp. 803–810.

POLYMER, BIOORGANIC, AND HYBRID NANOMATERIALS

Sulfonated Polyimide–Silica Composite Membranes: Preparation, Morphology and Proton Conductivity

M. Gupta[a,b], X. Zhu[a], A. P. Melnikov[c,d], K. R. Mugtasimova[c,e], A. V. Maryasevskaya[c,f], and D. A. Ivanov[c,d,f,g,*]

[a] *RWTH Aachen University, Aachen, Germany*
[b] *Indian Institute of Technology Delhi, New Delhi, India*
[c] *Moscow Institute of Physics and Technology, Dolgoprudny, Russia*
[d] *Lomonosov Moscow State University, Moscow, Russia*
[e] *Institute of General Physics, Moscow, Russia*
[f] *Institute of Problems of Chemical Physics, Chernogolovka, Russia*
[g] *Institut de Sciences des Matériaux de Mulhouse-IS2M, Mulhouse, France*
**e-mail: dimitri.ivanov.2014@gmail.com*

Received August 6, 2020; revised October 13, 2020; accepted October 13, 2020

Abstract—Sulfonated polyimides (SPIs)/silica composite membranes were prepared via an in situ sol–gel reaction followed by solution casting. SPIs based on 1,4,5,8-naphthalene tetracarboxylic dianhydride, 4,4'-diaminodiphenyl ether-2,2'-disulfonic acid and 4,4'-diaminodiphenyl ether have been chosen for the preparation of composite membranes due to their relatively high hydrolytic stability. Membranes varying in degree of sulfonation as well as silica content were characterized by FT-IR spectroscopy, thermal gravimetric analysis, transmission electron microscopy and impedance spectroscopy. It was found that the thermal and hydrolytic stability of membranes was enhanced by silica particles. Based on the morphological and conductivity data it is suggested that formation of a hydrogen bonded network of silanol groups of silica nanoparticles and sulfonic acid groups of the polymer matrix enhances the proton conductivity via the hopping mechanism of proton transport.

DOI: 10.1134/S1995078020050043

INTRODUCTION

The proton exchange membranes (PEM) for fuel cells (FCs) (PEMFCs) are widely considered to be promising energy conversion devices because of high power density, high efficiencies, fast start-up, and very low or zero emission at the point of use and thus can be viable in a number of areas, including transportation, residential (stationary) power and portable power [1–3]. Perflurosulfonic acids such as Nafion® are state-of-the-art electrolyte materials in PEMFC applications due to their excellent chemical, mechanical and thermal stability in addition to their high proton conductivity [4]. However, the application of this type of membrane is limited due to significant technical deficiencies such as reduction in conductivity at low humidity, high methanol permeability and high cost. Therefore, the development of new ionomeric materials with improved membrane properties and low price is an urgent need. Some of the most promising candidates being explored for their potential application as FC membranes are sulfonated polyimides (SPI), poly(ether ketone)s, poly(arylene ether sulfone)s, polybenzimidazoles, etc [5]. Aromatic polyimides based on naphthalic anhydrides are very important high performance materials due to their high thermal, fire, radiation and chemical resistance and excellent mechanical properties. Their properties meet very well the requirements for the PEM materials of FC systems [6–9]. Moreover, a number of sulfonated polyimides (SPIs) have been reported to be promising materials for PEMFC applications [10–15], but their hydrolytic stability and proton conductivity still have to be further improved.

The aim of this work is to improve further the performance of SPI membranes. The strategy we used is an introduction of disperse inorganic fillers into the organic polymer matrix [16].

Hydrophilic silica is a well-known additive for Nafion® membranes for the enhancement of the thermal stability and water retention properties at high operation temperature [17–24]. Silica containing composite membranes have also been prepared based on non-fluorinated polyelectrolytes [25–28]. In many cases such composite membranes showed an improved performance in high temperature in both direct methanol and hydrogen PEMFCs.

SPI based composite membranes were produced by adding nanosized fumed SiO_2 (Aerosil®) to a cross-linked SPI matrix [29]. In another paper, an in situ sol gel reaction using tetraethoxysilane (TEOS) and 3-aminopropyl triethoxysilane as the coupling agent in the SPI was realized [30]. The present paper will be focused on the preparation of SPI/silica composite membranes via a base-catalyzed hydrolysis/condensation of TEOS in the solutions of SPI and by subsequent solution casting. The effect of silica content on the properties of SPI with different sulfonation degrees such as thermal stability, morphology and proton conductivity will be discussed.

EXPERIMENTAL

4,4'-diaminodiphenyl ether (ODA), ammonia aqueous solution (28 vol %) and triethylamine (Et_3N), 1,4,5,8-Naphthalene tetracarboxylic dianhydride (NTDA), *m*-cresol, benzoic acid (99.5%, ACS grade), concentrated sulfuric acid (95%), fuming sulfuric acid (with 30% free SO_3), tetraethoxysilane (TEOS) (99%), dimethylsulfoxide (DMSO) (99.9%), methanol (99.8%) and acetone (99.5%) were used as received. NTDA was dried for 24 h at 160°C in vacuum prior to use. The other chemicals were used as received.

The synthesis of 4,4'-diaminodiphenyl ether-2,2'-disulfonic acid (ODADS) and homo- and co-polyimides based on it was carried out following a literature procedure [10]. To a 250 mL three-neck flask placed in an ice bath was added 5.00 g (25.0 mmol) of ODA followed by slow addition of 8.75 mL of concentrated sulfuric acid (95%) along with stirring. On complete dissolution of ODA, 12.5 mL of fuming sulfuric acid (with 30% SO_3) was slowly added to the flask. The reaction mixture was stirred at 0°C for 2 h and then slowly heated to 80°C and was maintained at this temperature for another 2 h. Afterwards, the reaction mixture was cooled to room temperature and poured dropwise into 50 g of crushed ice. The white precipitate obtained was filtered off and then re-dissolved in sodium hydroxide solution (2M). The basic solution was filtered, and the filtrate was acidified using concentrated hydrochloric acid. The white precipitate obtained on acidification was filtered off, washed with water and methanol successively, and dried under vacuum at 80°C for 24 h. 7.00g of white powder was obtained (yield: 78%); $T_m = 264.8$°C. IR (KBr, cm^{-1}): 3473, 2626, 1633, 1519, 1474, 1426, 1255, 1147, 1087, 1023, 907, 817, 704, 643. ^{1}H NMR spectrum (DMSO-d_6; Et_3N was added for dissolution in DMSO): 7.01 (*d, J* = 3 Hz, 2H), 6.75 (*d, J* = 8.7 Hz, 2H), 6.39 (*dd, J* = 3Hz, 2H). Elemental analysis Calcd.: C, 40.0; H, 3.3; N, 7.7.; Found: C, 38.0; H, 3.9; N, 7.4.

To synthesize NTDA–ODADS homopolyimide to a 250 mL completely dried 3-neck flask equipped with a magnetic stirrer, nitrogen inlet and a condenser, were added 1.080g (3.0 mmol) of ODADS, 10.0 mL of *m*-cresol, and 0.72 g (7.2 mmol) of triethylamine successively. After complete dissolution of ODADS, 0.804 g (3.0 mmol) of NTDA and 0.52 g (4.26 mmol) of benzoic acid were added. The mixture was stirred at room temperature for several minutes till it dissolved, and then heated at 80°C for 4 h, and then at 180°C for 20 h. After cooling to 100°C, additional 20 mL of *m*-cresol were added to dilute the highly viscous polymer solution. This diluted polymer solution was then precipitated by pouring it into 200 mL of acetone. The fibre like precipitate was separated by filtration followed by washing with acetone. Resulting polymer was dried under vacuum at 80°C for 24 h. The sample prepared here has been designated as SPI10.

To synthesize NTDA-ODADS-ODA copolymer, 0.72 g (2.0 mmol) of ODADS, 12.0 mL of *m*-cresol and 0.48 g (4.8 mmol) of triethylamine were successively added to a 250 mL completely dried 3-neck flask equipped with a magnetic stirrer, nitrogen inlet and a condenser. After complete dissolution of ODADS, 0.4 g (2.0 mmol) of nonsulfonated diamine (ODA), 1.072 g (4.0 mmol) of NTDA, and 0.68 g (5.6 mmol) of benzoic acid were added. The reaction mixture was stirred at room temperature for several minutes till it dissolved. Afterwards, it was heated at 80°C for 4 h, and then at 180°C for 20 h. After cooling to 100°C, an additional 25 mL of *m*-cresol was added to dilute the highly viscous polymer solution, which was precipitated by pouring it into 200 mL of acetone. The fibre like precipitate was separated by filtration followed by washing with acetone. Resulting polymer was dried under vacuum at 80°C for 24 h. Different copolymer samples were prepared using the same procedure by taking the molar ratio of ODADS : ODA as 3 : 1 and 1 : 1 in the initial feed, and the samples have been designated as SPI31 and SPI11, respectively.

Membranes in triethylammonium salt form of the homopolyimide NTDA-ODADS was prepared by casting its DMSO solutions (10 wt %) onto a glass plate using a casting knife. The glass substrates were cleaned by keeping in alkali bath for 2 h, then rinsing with aqueous HCl and finally washing with deionized water for several times. The resulting membranes were dried at 80°C for 10 h. The co-polyimide membranes were cast from their *m*-cresol solution (10 wt %) and, were dried at 120°C for 10 h. Composite membranes were prepared by the same casting the solutions but DMSO with TEOS and aqueous NH_3 solution (2 M) was used as the solvent. The amount of TEOS was varied to obtain different SiO_2 loadings in the membrane (5–20 wt %). For preparing composite co-polyimide membranes, instead of DMSO, *m*-cresol was used as the solvent and the cast membranes were dried at 120°C for 10 h, the rest procedure being the same. The as-cast membranes were soaked in methanol at 60°C for 1 h to remove the residual solvent. Proton exchange treatment was carried out by immersing these mem-

branes in 1.0 M hydrochloric acid at room temperature for 24 h. Protonated membranes were then thoroughly washed with ultrapure water and dried in vacuum at 150°C for 20 h. The thickness of the membranes was in the range 10–20 μm.

^{1}H-NMR spectra were obtained on a Bruker DPX 300 at 300 MHz. DMSO-d_6 was used as solvent with tetramethylsilane as internal standard. Fourier transform infrared (FT-IR) spectra were collected in the range of 500–4000 cm^{-1} using Thermo Nicolet Nexus 470 spectrophotometer equipped with DTGS detector using 100 signal-averaged scans at a resolution of 8 cm^{-1}. Each sample was in a form of thin film of polymer (25 × 10 mm) placed on a KBr disc.

A TG-209 thermal gravimetric analysis (TGA) instrument (Netzsch) was used to study the thermal stability of synthesized polymers and membrane samples in nitrogen flow from 30 to 700°C at a heating rate of 10°C/min.

The morphology of the membranes was investigated by means of Transmission Electron Microscopy (TEM) using the Zeiss Libra 120 TEM operated at 120 kV. In all the samples, the contrast between the inorganic phase and the polymer was sufficient for imaging.

The bulk proton conductivity of the membranes was measured by electrochemical impedance spectroscopy (EIS) via four probe method using the protocol, in which the conductivity is measured as a function of relative humidity (RH) at 100°C. The measurements were performed in the longitudinal direction of the membranes over a frequency range of 500 Hz to 500 kHz and at amplitude of 20mV, using the Electrochemical Workstation IM6 (Zahner-Elektrik Gmbh and Co. KG, Germany) connected to the "Membrane Conductivity and Single Cell Test System BT-552" (BekkTech, USA). The measurements were performed under a nitrogen flow of 500 standard cubic centimetres per minute (sccm) and pressure of 230 kPa.

RESULTS AND DISCUSSION

Degree of sulfonation (DS) as well as ion-exchange capacity (IEC) of the resulting sulfonated polyimides (SPIs) and percent weight loss for different SPIs are summarized in Table 1.

The chemical structure of SPIs prepared in this work was identified by FT-IR spectroscopy. Figure 1 shows the FT-IR spectrum of protonated homopolymer SPI10. In the FT-IR spectrum, the broad absorption band at 3400 cm^{-1} is assigned to the absorbed water in the sample. The absence of anhydride carbonyl peaks at 1780 and 1740 cm^{-1} confirms the completion of the imidization reaction. The broad bands at 1250 and 1081 cm^{-1} correspond to the stretching vibrations of sulfonic acid groups.

Table 1. Theoretical degree of sulfonation (DS), ion-exchange capacity (IEC) and weight loss (%) due to desulfonation of SPI

	SPI10	SPI31	SPI11
NTDA (mmol)	2	2	2
ODADS (mmol)	2	1.5	1.0
ODA (mmol)	0	0.5	1.0
DS (%)	100	75	50
IEC (meq/g)	3.37	2.71	1.95
Weight loss theoretical (wt %)	28.5	21.4	14.3
Weight loss by TGA (wt %)	23.1	18.8	11.9

TGA results for polyimide membranes in these different temperature ranges are summarised in Table 2. All the membranes showed a three-step degradation profile. As described in the literature [10, 15], the initial weight loss below 200°C corresponds to the elimination of absorbed water and solvent. At temperature above 200°C, desulfonation occurs until 450°C. It was observed that the mass loss in the temperature range 250–450°C, which was due to the loss of sulfonic acid groups, increased with increasing degree of sulfonation. Meanwhile, it was also found that with the increase in the silica loading from 5 to 20 wt %, the onset temperature of backbone degradation in general tended to grow, that implies the enhancement of the thermal endurance of these SPI membranes because of the silica inclusion.

The bulk morphology of SPI11/silica and SPI31/silica composite membranes was analysed by TEM, Figs. 2 and 3, respectively. In the SPI11 membranes containing 5 wt % SiO_2 the formation of small silica particles in the size range of 10 to 25 nm was observed, and the silica nanoparticles were homoge-

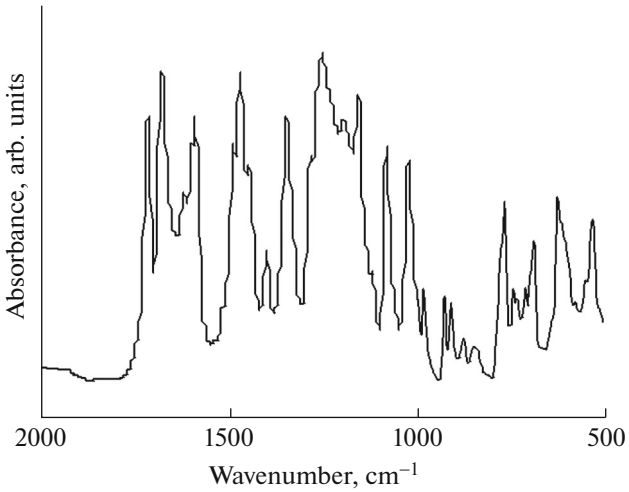

Fig. 1. FT-IR spectrum of sulfonated homopolyimide (SPI10).

Table 2. TGA results of membranes in nitrogen atmosphere and heating rate 10°C/min

	Mass Loss, %			Char Yield at 700°C (%)
	below 200°C	200–450°C	450–700°C	
SPI10	6.8	21.5	23.4	48.3
SPI10 + 5 wt %	4.6	24.8	24.7	45.9
SPI10 + 10 wt %	5.9	21.5	29.2	43.4
SPI10 + 15 wt %	6.3	17.6	24.2	51.9
SPI10 + 20 wt %	5.6	18.1	21.5	54.8
SPI31	4.5	18.0	22.6	54.9
SPI31 + 5 wt %	3.2	16.7	30.5	49.6
SPI31 + 10 wt %	7.2	21.6	29.8	41.4
SPI31 + 15 wt %	5.3	14.1	22.6	58.0
SPI31 + 20 wt %	6.3	15.3	22.9	55.5
SPI11	3.3	11.5	27.1	58.1
SPI11 + 5 wt %	3.2	15.8	30.7	50.3
SPI11 + 10 wt %	5.5	18.0	33.7	42.8
SPI11 + 15 wt %	3.1	11.8	28.5	56.6
SPI11 + 20 wt %	5.2	12.3	26.4	56.1

neously distributed in the SPI matrix. With the increase of silica content the particle size was found to grow and with high silica content (above 15 wt %) large particle agglomerations could be seen. In the SPI31 membranes at 10 wt % silica the particle size ranges from 15 to 70 nm, the membranes with 15 wt % SiO_2

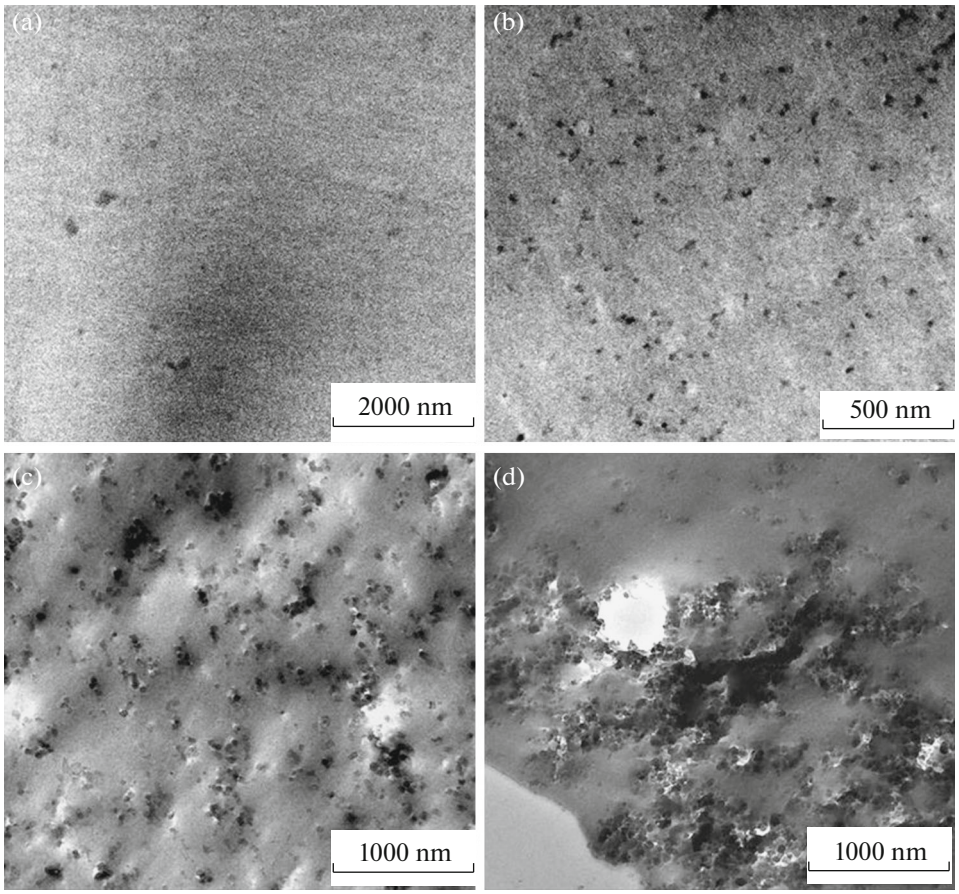

Fig. 2. TEM images of SPI11/silica composite membranes with (a) 5, (b) 10, (c) 15, and (d) 20 wt % silica.

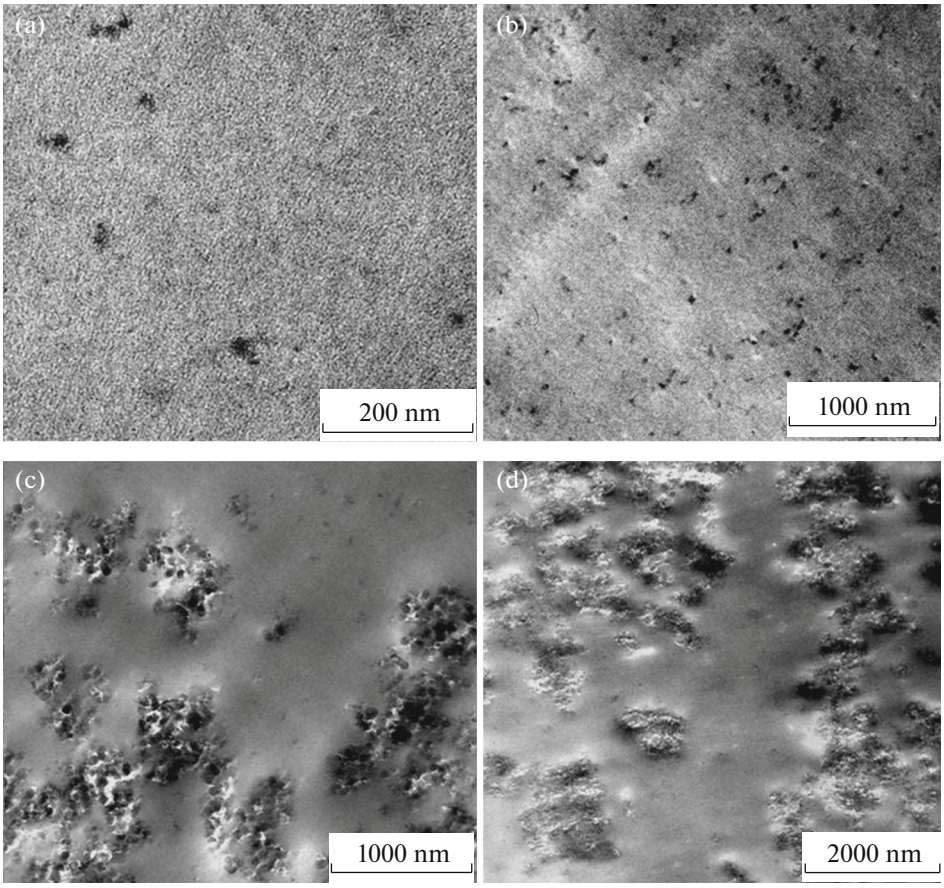

Fig. 3. TEM images of SPI31/silica composite membranes with (a) 5, (b) 10, (c) 15, and (d) 20 wt % silica.

content exhibited well distributed silica particles ranging from 20 to 60 nm. The silica particles derived from the basic hydrolysis/condensation of TEOS are hydrophilic; therefore, their compatibility with SPI matrices is reduced with the decrease in DS. This explains the formation of big agglomerates of silica particles in SPIs of lower DS at lower silica loading.

In Fig. 4 the proton conductivity σ of the SPI membranes is shown. The proton conductivity of these membranes was found to be strongly dependent on their IEC values and the RH. The SPI10 membrane has the highest IEC value. It is interesting to note that the conductivity of the SPI10 membrane at high RH is higher, but at low RH is lower than that of Nafion. Although all the co-polyimide membranes have much larger IEC values than Nafion 112 (IEC = 0.91 meq/g), their proton conductivity was found to be much lower compared to Nafion 112. This is most probably because Nafion membrane has a unique ionic channel structure, which is favourable for proton transport, whereas the present SPI membranes have a rather homogeneous structure [5, 10]. This structural discrepancy might also explain the different RH dependence of conductivity between the SPIs and Nafion.

It can be seen that the composite membranes exhibit a bit lower conductivity at all RH compared to membranes without SiO_2 content, Fig. 4. It is interesting to note that for all composite membranes having different DS the lowest proton conductivity value was observed at 5 wt % SiO_2 loading. It seems that at low silica loading these hydrophilic silica particles act merely as inert filler and thus decrease the effective IEC values of the membranes, resulting in the decrease in the proton conductivity. At high silica content the surface hydroxyl groups of particles start to form a hydrogen bonding network together with the sulfonic acid groups of the polymer matrix, which facilitates the hopping mechanism of the proton conductivity. However, certain irregularity was observed in the dependence of proton conductivity on the silica content. For example, the proton conductivity of the SPI10/silica composite membranes slightly decreases on going from 15 to 20 wt % SiO_2. For the series of the SPI11/silica composite membranes the proton conductivity slightly decreases on going from 10 to 15 wt % SiO_2 content, but again increases with 20 wt % SiO_2 content. This variation in proton conductivity can possibly be explained by the morphology of these membranes.

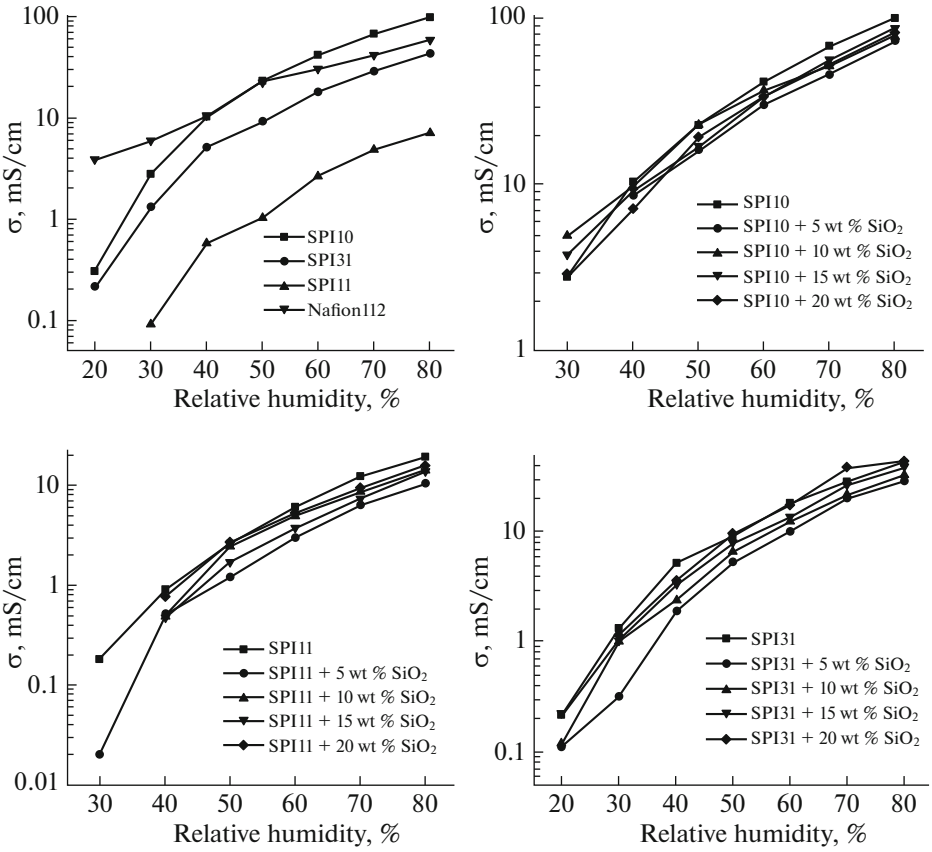

Fig. 4. Proton conductivity of SPI membranes having different degree of sulfonation and silica content as a function of relative humidity at 100°C.

The microstructure of SPI has been described by the presence of hydrophobic/hydrophilic phase separation. The hydrophobic domains are generated by the aromatic backbone, while the hydrophilic domains derive from the aggregation of sulfonic acid groups. Compared to Nafion®, the hydrophobic/hydrophilic phase separation of SPI is much less pronounced, resulting in narrower, less separated, highly branched and less interconnected hydrophilic channels passing through hydrophobic domains. Due to its microstructure, SPIs show lower proton conductivity at low hydration levels and stronger dependence of the proton conductivity on the content of water than Nafion® [9]. It is possible that the presence of hydrophilic silica nanoparticles influences the size, the interconnectivity and the degree of branching of the SPI hydrophilic channels thus offering new paths for the transport of protons.

It has been shown by TEM investigation that at higher silica loading big agglomerations of particles are present, resulting in tremendous increase in effective particle size that, ultimately, has detrimental effect on the proton conductivity. Indeed, if the proton transport occurs via a Grotthuss mechanism, i.e. via proton hopping along a hydrated network, the interfacial contact area between the ionomer and the silica filler should be as large as possible in order to enhance the conductivity, consequently, the size of the inorganic particles should be as small as possible. Therefore, the drop in conductivity at higher silica loadings for some composite samples can be attributed to the alteration of morphology due to the particle agglomeration.

The stability of the SPI membranes under fuel cell conditions was assessed by monitoring their behaviour during the conductivity measurement at 100% RH and 100°C. We found that the thermal and hydrolytic stability of the composite membranes increases with the increase of silica content till 10 wt %. At higher silica loadings, however, the composite membranes become less stable due to the increased brittleness. This may be due to the increase of the contribution of inorganic domains and particle agglomeration at higher silica loading.

CONCLUSIONS

Sulfonated polyimide/silica composite membranes with different degrees of sulfonation and silica loading based on the 1,4,5,8-naphthalene tetracarboxylic dianhydride, 4,4'-diaminodiphenyl ether-2,2'-disul-

fonic acid and 4,4'-diaminodiphenyl ether were successfully synthesized via an in situ sol–gel reaction using tetraethoxysilane as the silica precursor. The particle size of silica was found to be less than 100 nm. At low silica content, particles are homogeneously distributed in the polymer matrix, at high silica content, however, particle agglomeration was observed. Thermal and hydrolytic stability of the SPI membranes was improved by addition of silica particles till 10 wt % loading, higher silica loading, however, lead to the brittleness of the membrane and can be attributed to the increasing the interfacial contact area and can be explained by the formation of hydrogen bonding network of silanol groups on silica nanoparticles together with the sulfonic acid groups. Proton conductivity of composite membranes was found to be dependent on the particle distribution in the membranes. The membranes with smaller silica particles showed better proton conductivity than the ones containing large particle agglomerations. It can be concluded that addition of 10 wt % silica results in an optimal combination of proton conductivity and membrane stability.

FUNDING

The authors greatly thank the Ministry of Science and Higher Education of the Russian Federation (contract no. 05.605.21.0188 from 3 December 2019 (RFMEFI60519X0188)) for financial support.

REFERENCES

1. B. C. H. Steele and A. Heinzel, Nature (London, U.K.) **414**, 345 (2001).
2. F. Barbir and S. Yazici, Int. J. Energy Res. **32**, 369 (2008).
3. B. Smitha, S. Sridhar, and A. A. Khan, J. Membr. Sci. **259**, 10 (2005).
4. K. A. Mauritz and R. B. Moore, Chem. Rev. **104**, 4535 (2004).
5. M. A. Hickner, H. Ghassemi, Y. S. Kim, et al., Chem. Rev. **104**, 4587 (2004).
6. C. Genies, R. Mercier, B. Sillion, et al., Polymer **42**, 5097 (2001).
7. W. Jang, C. Lee, S. Sundar, et al., Polymer Degrad. Stab. **90**, 431 (2005).
8. N. Asano, M. Aoki, S. Suzuki, et al., J. Am. Chem. Soc. **128**, 1762 (2006).
9. Y. Yan, O. Yamada, K. Tanaka, and K. Okamoto, Polymer J. **38**, 197 (2006).
10. J. Fang, X. Guo, S. Harada, et al., Macromolecules **35**, 9022 (2002).
11. Y. Hongyan, K. Shi, N. Song, et al., Polymer **103**, 171 (2016).
12. C. Lee, S. Sundar, J. Kwon, and H. Han, J. Polym. Sci., Part A **42**, 3621 (2004).
13. J. Long, H. Yang, Y. Wang, et al., ChemElectroChem **7**, 937 (2020).
14. N. Ali, F. Ali, S. Saeed, et al., J. Mater. Sci.: Mater. Electron. **30**, 19164 (2019).
15. C. Genies, R. Mercier, B. Sillion, et al., Polymer **42**, 359 (2001).
16. C. I. Filipoi, X. Zhu, D. Turp, et al., Int. J. Hydrogen. Energy **37**, 14454 (2012).
17. S. T. Muntha, M. Ajmal, H. Naeem, et al., Polym. Compos. **40**, 1897 (2019).
18. K. T. Adjemian, R. Dominey, L. Krishnan, et al., Chem. Mater. **18**, 2238 (2006).
19. Z. G. Shao, P. Joghee, and I. M. Hsing, J. Membr. Sci. **229**, 43 (2004).
20. S. T. Muntha, J. Ambreen, M. Siddiq, et al., JTCM (2019).
21. R. A. Zoppi and S. P. Nunes, J. Electroanal. Chem. **445**, 39 (1998).
22. A. K. Sahu, G. Selvarani, S. Pitchumani, et al., J. Electrochem. Soc. **154**, B123 (2007).
23. K. T. Adjemian, S. Srinivasan, J. Benziger, and A. B. Bocarsly, J. Power Sources **109**, 356 (2002).
24. R. Jiang, H. R. Kunz, and M. J. Fenton, J. Membr. Sci. **272**, 116 (2006).
25. I. Colicchio, D. E. Demco, M. Baias, et al., J. Membr. Sci. **337**, 125 (2009).
26. Z. Gaowen and Z. Zhentao, J. Membr. Sci. **261**, 107 (2005).
27. P. Musto, G. Ragosta, G. Scarinzi, and L. Mascia, Polymer **45**, 1697 (2004).
28. S. Panero, P. Fiorenza, M. A. Navarra, et al., J. Electochem. Soc. **152**, A2400 (2005).
29. C. H. Lee, S. Y. Hwang, J. Y. Sohna, et al., J. Power Sources **163**, 339 (2006).
30. L. Zou, S. Roddecha, and M. Anthamatten, Polymer **50**, 3136 (2009).